HHS Public Access

Author manuscript

Biosens Bioelectron X. Author manuscript; available in PMC 2023 October 05.

Published in final edited form as:

Biosens Bioelectron X. 2023 September ; 14: . doi:10.1016/j.biosx.2023.100356.

Real-time temperature correction for magnetoresistive biosensors integrated with temperature modulator

Songeun Kim[a,b], **Shan X. Wang**[c,d], **Jung-Rok Lee**[a,b,*]

[a]Division of Mechanical and Biomedical Engineering, Ewha Womans University, Seoul, 03760, South Korea

[b]Graduate Program in Smart Factory, Ewha Womans University, Seoul, 03760, South Korea

[c]Department of Materials Science and Engineering, Stanford University, Stanford, CA, 93405, USA

[d]Department of Electrical Engineering, Stanford University, Stanford, CA, 93405, USA

Abstract

Magnetoresistance-based biosensors utilize changes in electrical resistance upon varying magnetic fields to measure biological molecules or events involved with magnetic tags. However, electrical resistance fluctuates with temperature. To decouple unwanted temperature-dependent signals from the signal of interest, various methods have been proposed to correct signals from magnetoresistance-based biosensors. Yet, there is still a need for a temperature correction method capable of instantaneously correcting signals from all sensors in an array, as multiple biomarkers need to be detected simultaneously with a group of sensors in a central laboratory or point-of-care setting. Here we report a giant magnetoresistive biosensor system that enables real-time temperature correction for individual sensors using temperature correction coefficients obtained through a temperature sweep generated by an integrated temperature modulator. The algorithm with individual temperature correction coefficients obviously outperformed that using the average temperature correction coefficient. Further, temperature regulation did not eliminate temperature-dependent signals completely. To demonstrate that the method can be used in biomedical applications where large temperature variations are involved, binding kinetics experiments and melting curve analysis were conducted with the temperature correction method. The method

*Corresponding author. Division of Mechanical and Biomedical Engineering, Ewha Womans University, Seoul, 03760, South Korea. jungrok@ewha.ac.kr (J.-R. Lee).

Declaration of competing interest

The authors declare the following financial interests/personal relationships which may be considered as potential competing interests: S.X.W. has related patents or patent applications assigned to Stanford University and out-licensed for potential commercialization. S.X.W. has stock or stock options in MagArray, Inc., which has licensed relevant patents from Stanford University for commercialization of GMR biosensor chips.

CRediT authorship contribution statement

Songeun Kim: Methodology, Validation, Formal analysis, Visualization. **Shan X. Wang:** Supervision, Resources, Writing – review & editing. **Jung-Rok Lee:** Conceptualization, Supervision, Funding acquisition, Writing – original draft.

Appendix A. Supplementary data

Supplementary data to this article can be found online at https://doi.org/10.1016/j.biosx.2023.100356.

successfully removed all temperature-dependent artifacts and thus produced more precise kinetic parameters and melting temperatures of DNA hybrids.

Keywords

Magnetoresistance; Temperature compensation; GMR biosensors; Thermoelectric effect; Kinetics; Melting curve analysis

1. Introduction

Magnetoresistance-based magnetic biosensors have been developed for the highly sensitive detection of various biomolecules (Gaster et al., 2009; Graham et al., 2003; Ren et al., 2020). These biosensors typically employ the effect of anisotropic magnetoresistance (AMR) in a simple structure (Graham et al., 2004; Rizzi et al., 2014) or giant magnetoresistance (GMR) in a multilayered structure (Lee et al., 2016; Wang et al., 2015). Due to the lack of magnetic contents in most biological samples, magnetic biosensors can achieve high sensitivities for many biomarkers (Gaster et al., 2009; Lee et al., 2018; Ren et al., 2020). However, since magnetoresistance-based biosensors rely on electrical resistance changes upon an external magnetic field, they are inevitably vulnerable to temperature changes. Thus, introducing buffer solutions or biological samples at different temperatures could induce artifacts in measurement signals. Further, if the temperature fluctuates during measurement, biosensors exhibit undesirable signals disturbed by temperature changes, which would be significantly difficult to be separated from the signals induced by target biomarkers. In addition, as the applications of magnetic biosensors spread into various biomedical fields, not only to obtain consistent results for end-point measurements in immunoassays (Gao et al., 2019; Wu et al., 2017) or DNA microarrays (Ravi et al., 2022), to regulate or modulate the temperature also becomes more important. For example, some magnetic biosensors detect DNA mutations using melting curve analysis where the temperature is swept in a wide range during measurement (Rizzi et al., 2017). Another emerging application of magnetic biosensors is kinetics measurement where all kinetic parameters vary with temperature because they are thermodynamic properties (Decherchi and Cavalli, 2020; Gaster et al., 2011; Lee et al., 2016).

The easiest solution to controlling temperature is to include an enclosure surrounding the biosensors. However, this manipulation of the sensor environment is ineffective because local temperature changes at the surfaces of the biosensors would mainly influence the signals. As demonstrated in this study, even regulating the local temperature with an extra device cannot completely remove the artifacts introduced by adding buffers at different temperatures. In addition, given that a small amount of current is always applied to magnetoresistance-based biosensors to read out electrical resistance changes, the magnetoresistance-based biosensors inherently produce heat locally (Kim et al., 2018). Therefore, instead of controlling the temperature globally, monitoring local temperatures and compensating signals for them would be amongst the most effective.

Previous studies suggested using sensors' nominal resistance changes to monitor the averaged local temperature around their surfaces (Hall et al., 2010b). However, the algorithm

requires adding a cold solution, such as isopropanol alcohol at −20 °C, to significantly modulate the temperature. Due to variations in the fabrication process, different sensor chips have different responses to temperature changes (i.e., temperature coefficients). Therefore, to calibrate temperature coefficients for each sensor chip, a cold nonaqueous solution has to be repeatedly added to each chip, which might cause contamination or damage the probes on the sensors. In addition, since the algorithm estimates the average temperature coefficient over many sensors on a chip, variations in temperature coefficients across the sensors are not completely corrected.

In this regard, we herein report a real-time temperature correction method to precisely remove artifacts induced by temperature changes from magnetic biosensors' signals using a built-in temperature modulator. To demonstrate the effectiveness of the method, GMR biosensors were used to build up a system integrated with the temperature modulator. Among various magnetic biosensors, GMR biosensors have shown high sensitivities in many applications, including kinetics measurement (Lee et al., 2016) and melting curve analysis (Rizzi et al., 2017) where temperature changes are greatly involved. Further, since GMR biosensors have already been fabricated in sensor arrays (Osterfeld et al., 2008), a temperature correction method applicable to multiple sensors on the same chip is considerably needed. With the method, we successfully corrected signals from multiple sensors on a chip and different chips without adding any extra solution to chips or requiring user involvement, and demonstrated that a binding curve between streptavidin and biotin and the melting curves of DNA hybrids could be effectively compensated to obtain more precise kinetic parameters and melting temperatures, respectively.

2. Materials and methods

2.1. Materials and instruments

Phosphate-buffered saline (PBS) at pH 7.4, bovine serum albumin (BSA), and biotinylated BSA were purchased from Thermo Fisher. Purified water was obtained using a Direct-Q3 UV water purification system (Merck, Germany). Streptavidin-coated magnetic nanoparticles (MNPs) were purchased from Miltenyi Biotec (Germany). Temperature controlling systems were developed in combination with temperature controllers from Wavelength Electronics (USA). GMR biosensor signals were measured using a custom-made reader station, and the deposition of reagents onto GMR biosensors was performed with a noncontact robotic arrayer (SciFlexArrayer S3; Scienion, Germany). The reader system and temperature controller were controlled by custom-developed programs based on LabVIEW (National Instruments, USA).

2.2. GMR biosensors with a temperature modulator

GMR biosensors consist of multiple nanoscale layers of magnetic and nonmagnetic materials, as described previously (Gaster et al., 2009; Kim et al., 2022). GMR biosensors with a stack of seed layer/IrMn (8)/CoFe (2)/Ru (0.8)/CoFe (2)/Cu (2.3)/CoFe (4.5)/capping layer (all thickness in nm) were fabricated in a 10 × 8 array on a silicon die (chip). They were mounted on a printed circuit board (PCB) that contains a hole through which the backside of the chip is accessible. The chip was assembled with a custom-designed cartridge

equipped with a resistance temperature detector (RTD) and thermoelectric cooler (TEC). A reaction well over the GMR biosensors was created through an opening in the top part of the cartridge. RTD and TEC were connected to the temperature controller to modulate the temperatures of the GMR biosensors via a feedback loop.

2.3. Temperature correction

To obtain temperature correction coefficients (κ) of all GMR biosensors on the same chip, the temperature of the GMR biosensor cartridge was automatically swept from 25 °C to 3.5 °C with a sweeping rate of ~0.1 °C s^{-1} using a custom program before any measurement while the signals of 80 GMR biosensors were being simultaneously recorded. With a double modulation scheme reported previously (Hall et al., 2010a), the GMR biosensor signals were analyzed in the frequency domain to acquire a carrier-tone (CT) signal at a frequency of current applied to the sensors and two side-tone (ST) signals at frequencies that are a frequency of magnetic field applied to the sensors apart from the CT frequency. CT and ST signals recorded over the temperature sweep were used to calculate the temperature correction coefficients.

2.4. Validation of temperature correction

The custom-developed programs were designed to show temperature-corrected and uncorrected signals for comparison. To investigate the effectiveness of the temperature correction method, the temperature modulator was turned off after the temperature correction coefficients were obtained with 200 μL of purified water in the reaction well. After the baseline signals were obtained, either 100 μL of purified water at 4 or 40 °C was added to the reaction well. In addition, another experiment with the same solutions was performed while the temperature was maintained at 30 °C using the temperature modulator to observe the effect of temperature regulation together with the temperature correction method.

2.5. Decoupling of temperature artifacts from binding curves

To observe binding signals, half of the GMR sensors were coated with biotinylated BSA, and the other half was treated with BSA as a negative control. The GMR sensors were prepared with a previously reported protocol (Kim et al., 2022). Briefly, a GMR sensor chip was washed twice with acetone, methanol, and isopropanol. Approximately 2 nL of biotinylated BSA at 2 mg mL^{-1} and BSA at 10 mg mL^{-1} were deposited on the GMR sensors, respectively, using a noncontact arrayer. The GMR biosensor chip was stored in a humid chamber at 4 °C overnight. The chip was assembled with the cartridge, washed twice with a washing buffer (PBS with 0.1% BSA and 0.05% Tween 20), and incubated with 1% BSA for 1 h at room temperature. The chip was then washed again with the washing buffer, and inserted into a reader system. After the temperature correction coefficients were measured and the baseline signals were obtained, the washing buffer inside the reaction well was removed and 100 μL of purified water at 4 °C was injected into the well using a chilled pipette tip. Once the temperature of the sensors reached a thermal equilibrium state, the purified water inside the well was removed, and 70 μL of MNPs at 4 °C were injected into the well with a chilled pipette tip. The concentration of MNPs was approximately 1 nM (Lee et al., 2016).

2.6. Curve fitting of binding kinetics

To obtain kinetic parameters from binding curves, a curve fitting algorithm was developed using nonlinear regression algorithms in MATLAB (MathWorks, USA). The first 10 min data after MNP injection were taken to fit the data for a simple exponential function, $y = A \bullet [1 - \exp(-B \bullet t)]$.

2.7. Decoupling of temperature artifacts from the melting curves

To obtain the melting curves of DNA hybrids, GMR sensors were functionalized with two different DNA probes (P1 and P2) with duplicates after washed with acetone, methanol, and isopropanol. Each probe at 20 μM was prepared in a 2 × saline-sodium citrate (SSC) buffer solution, and deposited on the GMR sensors using a noncontact arrayer. BSA was immobilized on different sensors as a negative control. After overnight incubation at 4 °C, the GMR sensor chip was washed with the washing buffer, and incubated with 1% BSA for 1 h at room temperature with agitation. The chip was incubated with pure water for 1 h at 37 °C. Then, the chip was washed with the 2 × SSC buffer solution and incubated with a biotinylated target DNA at 1 μM in 2 × SSC for 1 h at room temperature with agitation. The chip was finally washed with the 2 × SSC buffer solution and inserted into the reader system, while the temperature of the modulator was set to 20 °C. After the temperature correction coefficients and the baseline signals were obtained, 70 μL of MNPs were added to the reaction well. Then, after the signals were all saturated, the chip was washed with the 2 × SSC buffer solution. To obtain the melting curves, the temperature was swept from 20 °C to 50 °C.

3. Results and discussion

GMR biosensors were fabricated in an array of 10 × 8 on a single chip and based on the quantum mechanical effect of GMR to detect an external magnetic field (Fig. 1a). Since GMR biosensors can sense a minute magnetic field from MNPs, target molecules or binding events can be detected on individual sensors by labeling target molecules with MNPs. To control the temperature of each sensor, a built-in temperature modulator consisting of TEC and RTD was integrated into the cartridge of the GMR biosensor chip (Fig. 1b). The modulator was mounted in proximity to the chip, and a thermally conducting connection was generated to change or maintain the local temperature of the sensor effectively (Fig. 1c). To obtain signals from each sensor, the cartridge was inserted into a custom-made reader station equipped with a set of electronics and a Helmholtz coil that can apply an external magnetic field to the chip (Fig. 1d). While an AC magnetic field was applied at a frequency of 90 Hz, AC voltages at a frequency of 500 Hz were applied to the sensors to read out magnetoresistance signals related to the existence of MNPs near the sensors (see details in Supplementary Information). Due to this double-modulation scheme, two types of signals in the frequency domain can be acquired. Whereas the CT signal at 500 Hz includes information on the nominal resistance, the ST signals at 410 and 590 Hz carry both magnetoresistance and nominal resistance information (Fig. S1). Since the nominal resistance varies with temperature, the local temperature of the sensor can be monitored using CT signals. Then, ST signals can be corrected to obtain temperature-independent magnetoresistance signals. The ratio of magnetoresistance to nominal resistance is defined

as magnetoresistance ratio (MR), and GMR biosensor signals are typically reported as MR. The temperature modulator was connected to a temperature controller, and the reader station and temperature controller were communicated with data acquisition (DAQ) boards (Fig. 1e).

3.1. Temperature correction procedure

To estimate temperature correction coefficients, the temperature has to be modulated within a range that the sensors typically experience during the measurement. The temperature of typical biological samples ranges from 0 to 40 °C, but if melting curve analysis or polymerase chain reaction (PCR) is involved the sensors are confronted with up to 90 °C. Although a wider sweep of temperature modulation will result in more accurate temperature correction coefficients, it might cause denaturation or degradation of probes on the sensors, especially protein-based probes. Thus, we determined that the temperature of the sensor chip is swept using the temperature modulator from 25 °C down to 3.5 °C. To demonstrate that the modulator works properly, the actual temperature was monitored by RTD as well as ST and CT signals simultaneously while the reaction well was filled with 200 μL of purified water (Fig. 2a). The actual temperature followed the set temperature fairly, meaning the feedback control was performed properly. Since ST and CT signals are temperature-dependent, they varied linearly with the temperature (Fig. 2a). The prompt responses in ST and CT signals shown in Fig. 2a indicate that heat transfer through the cartridge was effective enough and that the local temperature around the sensor immediately responded to the changes. Thus, it was proven that the local temperature could be monitored using ST and CT signals. In addition, since the temperature coefficient of resistance (α) in the GMR sensor was positive, CT signals became higher as the temperature was getting lower, which was expected by a mathematical model (see details in Supplementary Information). The mathematical model also predicted that if the temperature coefficient of magnetoresistance (β) is greater than the doubled temperature coefficient of resistance (i.e., $\beta > 2\alpha$), ST signals will be higher as the temperature goes down, again confirmed by observed data. Using ST and CT signals obtained from this automatic temperature sweep, the temperature correction coefficients (κ) can be estimated by calculating the slope in the graph of processed ST versus CT signals as defined in the following equation:

$$\kappa \triangleq \frac{\left(\frac{ST(t)}{ST(0)} - 1\right)}{\left(\frac{CT(t)}{CT(0)} - 1\right)} = \frac{(\beta - 2\alpha)\Delta T}{-\alpha \Delta T} = \frac{\beta - 2\alpha}{-\alpha} \quad (1)$$

where ST(t) and CT(t) are ST and CT signals acquired over the temperature sweep, respectively, and ST (0) and CT (0) are the initial ST and CT signals, respectively.

All pairs of processed ST and CT from 80 sensors on a chip are shown in Fig. 2b. With the method proposed in this study, the continuous sweep of temperature was able to generate almost equally-spaced data sets which can improve the accuracy of prediction on temperature correction coefficients, compared to the addition of a cold solution which typically induces a spike in temperature (i.e., unevenly distributed data). In Fig. 2b, the average of temperature correction coefficients can be obtained and used to compensate for

temperature changes as proposed in previous studies (Hall et al., 2010b). Since there were significant variations in temperature correction coefficients across the sensors on the same chip (Fig. 2c), using the average value was ineffective in correcting signals from all sensors. Further, due to batch-to-batch variations, chips from different batches showed highly diverse temperature correction coefficients (Fig. 2d). Therefore, temperature correction coefficients should be evaluated for all sensors whenever a new sensor chip is used for any measurement.

3.2. Validation of temperature correction

Once the temperature correction coefficients are obtained, the signals afterward can be instantaneously corrected to show temperature-independent signals. However, to demonstrate the effectiveness of correction on individual sensors, the signals corrected with the average of temperature correction coefficients were also recorded together with uncorrected signals. To validate the method, cold (4 °C) or hot (40 °C) water was intentionally added to the chips to disturb the temperature around the sensors. In Fig. 3a, these sudden changes induced enormous spikes in signals without any correction. Whereas the correction with the average of temperature correction coefficients showed outstanding performance in eliminating temperature-induced signals, individual correction using each sensor's temperature correction coefficient rendered even better outcomes. Due to the excellent effectiveness of the individual correction, the signal spreading (±7.3 ppm in MR) in the sudden spike regions was similar to the background noise level (±6.1 ppm in MR) compared to the correction with the average value (±10.5 ppm in MR), as shown in Fig. 3b. The correction with the average value could be still preferred and used for different chips after the one-time acquisition with one chip because of its ease of implementation and marginal benefits provided by the individual correction. However, due to high batch-to-batch variations as shown in Fig. 2d, the average values from different chips are greatly diversified. Thus, applying the average temperature correction coefficient obtained from one chip to another from a similar batch resulted in quite deviated signals (Fig. 3c and d) and even applying it to a distinct batch completely distorted the signals (Fig. 3c and e). These results clearly demonstrated the need to develop a method that can be carried out every time for any chip to estimate temperature correction coefficients without harming the sensors or probes.

3.3. Temperature correction under regulated temperature

Whereas the temperature modulator was designed to sweep the temperature to obtain temperature correction coefficients, it could also be used to maintain the temperature constant to prevent external disruption from affecting the signals. This approach might be considered as a means to remove the complex algorithm of temperature correction when the measurement is only performed at a constant temperature. However, if the measurement is involved with reagents at different temperatures or intentional changes in temperature, for example, in melting curve analysis, this approach cannot be realized. To support the argument, the temperature modulator was used to keep the temperature constant at 30 °C after all temperature correction coefficients had been obtained. Again, cold or hot water was added to the chip to disturb the temperature around the sensors while the temperature was maintained. Due to active temperature regulation, the uncorrected signals went back to baselines much faster after their peaks compared to the case where the modulator was off

(Figs. 3a and 4), meaning the temperature around the sensors went back much faster to the temperature at which the baseline signals were measured. In addition, before adding water at different temperatures, there were small drops in the uncorrected signals in response to the aspiration of solution left in the reaction well. Because the aspiration disturbed thermal equilibrium (cooling the sensors), the modulator attempted to increase the temperature rapidly and overshot the target, resulting in signal drops, not rises. Thus, only signal drops were observed during the aspiration regardless of whether cold or hot water was added after the aspiration (Fig. 4). The temperature correction with either individual temperature correction coefficients or their average effectively compensated for temperature changes, but again the former showed better performance (Fig. 4). As demonstrated in this study, maintaining the temperature constant with the modulator was not practical to eliminate the temperature disruption because local disturbance affected the signals much faster compared to the speed of feedback control on the temperature. Rather, temperature correction could remove all artifacts due to temperature changes, especially with individual temperature correction coefficients.

3.4. Correction on binding kinetics

After finding that the individual temperature correction outperforms, the method was applied to the kinetics measurement to confirm that it can be used in a biomedical application. As a model system, bindings between streptavidin and biotin were measured with GMR biosensors. Biotinylated BSA was immobilized on half of the 80 sensors, and BSA was coated on the other half as a negative control (Fig. S2). When streptavidin-coated MNPs are introduced to the chip where biotinylated BSA and BSA are immobilized, it is expected that MNPs will only bind to the biotinylated BSA-coated sensors and generate binding signals (Fig. 5a). However, if the temperature of the MNP solution is not the same as that of the chip, binding signals will be coupled with artifacts due to temperature changes. To demonstrate that the method can effectively decouple the binding signals from temperature-dependent signals, cold water at 4 °C without any MNP was added to the chip first. Then, an MNP solution at 4 °C was added to the chip (Fig. 5b). Again, uncorrected signals were intentionally recorded for comparison. In the uncorrected signals, sudden spikes were observed in biotinylated BSA and BSA sensors when cold water was added. However, when the MNP solution was introduced, the same spike pattern was only observed in BSA-coated sensors, meaning no MNP was bound to the sensors. From the biotinylated BSA sensors, the spike signals and binding signals were coupled together, so it was quite difficult to separate the binding signals from others. With the correction method, temperature-dependent signals can be all corrected and the results clearly showed only binding curves (Fig. 5c). Based on the corrected signals, kinetic parameters were estimated using the Langmuir isotherm and nonlinear curve fitting algorithm. Kinetic parameters, including dissociation rate constant (k_{off}) and association rate constant (k_{on}), are important factors in analyzing the kinetics of streptavidin and biotin interactions. However, their dissociation rate constant is typically assumed to be negligible because it is relatively much smaller than the product of the association rate constant and the ligand concentration (in this case, the concentration of MNPs) (Gaster et al., 2011). Therefore, the observed binding curve is only determined by their product, and the association rate constant can be calculated from the exponent of the fitted curve (Fig. 5d). Using the concentration of the MNPs, the association rate constant

was 6.8×10^6 M^{-1} s^{-1}, in agreement with the typical values ranging from 3.0×10^6 to 4.5×10^7 M^{-1} s^{-1} (Srisa-Art et al., 2008).

3.5. Correction on melting curve analysis

Another biomedical application where temperature correction is greatly needed is melting curve analysis because the signals are heavily affected by a wide sweep in the temperature (Rizzi et al., 2014, 2017). To demonstrate the effectiveness of the temperature correction algorithm in melting curve analysis, we immobilized two oligonucleotide probes (P1 and P2) that can be hybridized with a kind of biotinylated target oligonucleotide (T) with different degrees of affinities on different GMR biosensors along with BSA as a negative control (Fig. 6a). The detailed information on the probes and target is shown in Table S1. After the target oligonucleotide was incubated with the chip, the chip was measured on the reader system by adding MNPs to the reaction well (Fig. 6b). As MNPs have bound to the biotin on the target oligonucleotides that already formed hybrids with the probes on the sensors, signals from the sensors were increasing and eventually saturated. Once the signals were saturated, unbound MNPs were washed with a 2 × SSC buffer solution, and the temperature of the chip slowly increased up to 50 °C to obtain melting curves (Fig. 6c). Again, although the system reported temperature-corrected signals automatically, we intentionally recorded uncorrected signals together during measurement for comparison. Without temperature correction, large downward signals due to the temperature rise were observed from all sensors during the melting process, and they were hardly differentiated from the melting curves (Fig. 6d). Especially, such monotonically decreasing signals from the BSA-coated sensors proved that the majority of such signals is solely a temperature-induced portion. Obviously, small bumps in the signals were observed due to the addition of cold MNPs and washing, as expected (Fig. 6d). Through temperature correction, temperature-dependent signals were all removed and melting curves were clearly obtained (Fig. 6e). To identify the melting temperatures of hybrids from melting curves more precisely, melting peaks are commonly estimated from the curves via differentiation (Azbel, 1979). The inverted first-order derivatives of uncorrected and corrected signals were calculated to see if only differentiation of the signal can improve the accuracy of prediction on melting temperature, although there are huge artifacts due to the wide temperature sweep (Fig. 6f and g). The melting temperatures estimated from the uncorrected signals were 33.9 °C and 30.4 °C for P1 and P2 hybrids with T, respectively. In contrast, the corrected signals estimated the melting temperatures as 36.3 °C and 29.9 °C for P1 and P2 hybrids with T, respectively. The melting temperatures estimated with the corrected signals were much closer to the theoretically predicted values, which are 36.7 °C and 28.9 °C for P1 and P2 hybrids with T, respectively, using one of the most accurate simulation tools (Markham and Zuker, 2005). Thus, the temperature correction algorithm along with differentiation was capable of estimating the melting temperatures of DNA hybrids on GMR biosensors through the melting curve analysis more accurately. In addition, we investigated the reproducibility of the melting curve analysis by measuring the melting temperature with triplicate sensors on three different days to estimate the coefficient of variation (CV). The CV estimated for a DNA duplex was 0.98% (Fig. S3).

4. Conclusions

The signals of magnetoresistance-based biosensors are affected by changes in temperature. To separate target or biological event-induced signals from temperature-dependent artifacts, we developed a highly effective system that can correct signals from all GMR biosensors using individual temperature correction coefficients. As a panel of biomarkers has been used to diagnose a disease or determine one's health condition (Lara et al., 2015; Piratvisuth et al., 2022), an array of biosensors that can measure multiple biomarkers at a time would be more desirable in the future. In this regard, the temperature correction method capable of fine-tuning each sensor using individual temperature correction coefficients would be truly beneficial to develop next-generation biosensors. Further, maintaining ambient temperature constant still produced unwanted artifacts in the signals, which clearly showed the necessity of local temperature monitoring and individual correction. Another merit of this temperature correction method is that this technique can automatically provide recalibrated temperature correction coefficients for each use of new sensors without damaging the sensor or requiring additional user involvement. Many studies have reported methods with preset temperature correction coefficients (Hall et al., 2010b; Jang et al., 2018), but the technique in this study enables instantaneous correction with recalibrated temperature correction coefficients which can facilitate the accurate reading of signals in real-time under point-of-care (POC) settings. However, to use the method for such applications, the temperature modulator could be redesigned with more energy-efficient components, such as resistive heaters, to minimize power consumption. In addition, a faster temperature sweeping rate to obtain temperature correction coefficients can reduce operation time and save energy with minimal errors in calculation. Lastly, we anticipate that this method can be implemented in other types of magnetoresistance-based biosensors. Further, when GMR sensors are used as a magnetometer, this technique could enable a more precise measurement of a magnetic field with a large deviation in temperature.

Supplementary Material

Refer to Web version on PubMed Central for supplementary material.

Acknowledgments

This work was supported by the National Research Foundation of Korea (NRF) grants funded by the Korean government (NRF-2019M3C1B8090804, NRF-2019R1F1A1062638, NRF-2020R1C1C1 005416, and NRF-2023R1A2C1006611) and the National Institutes of Health (NIH) grants (1R01CA257843 and 1R21DK131776).

Data availability

Data will be made available on request.

References

Azbel MY, 1979. Proc. Natl. Acad. Sci. U.S.A. 76 (1), 101–105. [PubMed: 284324]

Decherchi S, Cavalli A, 2020. Chem. Rev. 120 (23), 12788–12833. [PubMed: 33006893]

Gao Y, Huo WS, Zhang L, Lian J, Tao W, Song C, Tang JP, Shi S, Gao YH, 2019. Biosens. Bioelectron. 123, 204–210. [PubMed: 30174274]

Gaster RS, Hall DA, Nielsen CH, Osterfeld SJ, Yu H, Mach KE, Wilson RJ, Murmann B, Liao JC, Gambhir SS, Wang SX, 2009. Nat. Med. 15 (11), 1327–1332. [PubMed: 19820717]

Gaster RS, Xu L, Han SJ, Wilson RJ, Hall DA, Osterfeld SJ, Yu H, Wang SX, 2011. Nat. Nanotechnol. 6 (5), 314–320. [PubMed: 21478869]

Graham DL, Ferreira HA, Freitas PP, 2004. Trends Biotechnol. 22 (9), 455–462. [PubMed: 15331226]

Graham DL, Ferreira HA, Freitas PP, Cabral JMS, 2003. Biosens. Bioelectron. 18 (4), 483–488. [PubMed: 12604266]

Hall DA, Gaster RS, Lin T, Osterfeld SJ, Han S, Murmann B, Wang SX, 2010a. Biosens. Bioelectron. 25 (9), 2051–2057. [PubMed: 20207130]

Hall DA, Gaster RS, Osterfeld SJ, Murmann B, Wang SX, 2010b. Biosens. Bioelectron. 25 (9), 2177–2181. [PubMed: 20219342]

Jang C, Park JK, Lee HJ, Yun GH, Yook JG, 2018. Sensors 18 (11), 3850. [PubMed: 30423976]

Kim K, Hall DA, Yao CY, Lee JR, Ooi CC, Bechstein DJB, Guo Y, Wang SX, 2018. Sci. Rep. 8, 16493. [PubMed: 30405155]

Kim S, Kim J, Im J, Kim M, Kim T, Wang SX, Kim D, Lee JR, 2022. Microchim. Acta 189 (7), 256.

Lara J, Cooper R, Nissan J, Ginty AT, Khaw KT, Deary IJ, Lord JM, Kuh D, Mathers JC, 2015. BMC Med. 13, 222. [PubMed: 26373927]

Lee JR, Appelmann I, Miething C, Shultz TO, Ruderman D, Kim D, Mallick P, Lowe SW, Wang SX, 2018. Theranostics 8 (5), 1389–1398. [PubMed: 29507628]

Lee JR, Bechstein DJB, Ooi CC, Patel A, Gaster RS, Ng E, Gonzalez LC, Wang SX, 2016. Nat. Commun. 7, 12220. [PubMed: 27447090]

Markham NR, Zuker M, 2005. Nucleic Acids Res. 33, W577–W581. [PubMed: 15980540]

Osterfeld SJ, Yu H, Gaster RS, Caramuta S, Xu L, Han SJ, Hall DA, Wilson RJ, Sun SH, White RL, Davis RW, Pourmand N, Wang SX, 2008. Proc. Natl. Acad. Sci. U.S.A. 105 (52), 20637–20640. [PubMed: 19074273]

Piratvisuth T, Tanwandee T, Thongsawat S, Sukeepaisarnjaroen W, Esteban JI, Bes M, Kohler B, He Y, Swiatek-de Lange M, Morgenstern D, Chan HLY, 2022. Hepatol. Commun. 6 (4), 679–691. [PubMed: 34796691]

Ravi N, Chang SE, Franco LM, Nagamani SCS, Khatri P, Utz PJ, Wang SX, 2022. Biosens. Bioelectron. 205, 114086. [PubMed: 35192997]

Ren CH, Bayin QG, Feng SL, Fu YS, Ma X, Guo JH, 2020. Biosens. Bioelectron. 165, 112340. [PubMed: 32729483]

Rizzi G, Lee JR, Dahl C, Guldberg P, Dufva M, Wang SX, Hansen MF, 2017. ACS Nano 11 (9), 8864–8870. [PubMed: 28832112]

Rizzi G, Osterberg FW, Dufva M, Hansen MF, 2014. Biosens. Bioelectron. 52, 445–451. [PubMed: 24094523]

Srisa-Art M, Dyson EC, Demello AJ, Edel JB, 2008. Anal. Chem. 80 (18), 7063–7067. [PubMed: 18712935]

Wang Y, Wang W, Yu LN, Tu L, Feng YL, Klein T, Wang JP, 2015. Biosens. Bioelectron. 70, 61–68. [PubMed: 25794959]

Wu K, Klein T, Krishna VD, Su DQ, Perez AM, Wang JP, 2017. ACS Sens. 2 (11), 1594–1601. [PubMed: 29068663]

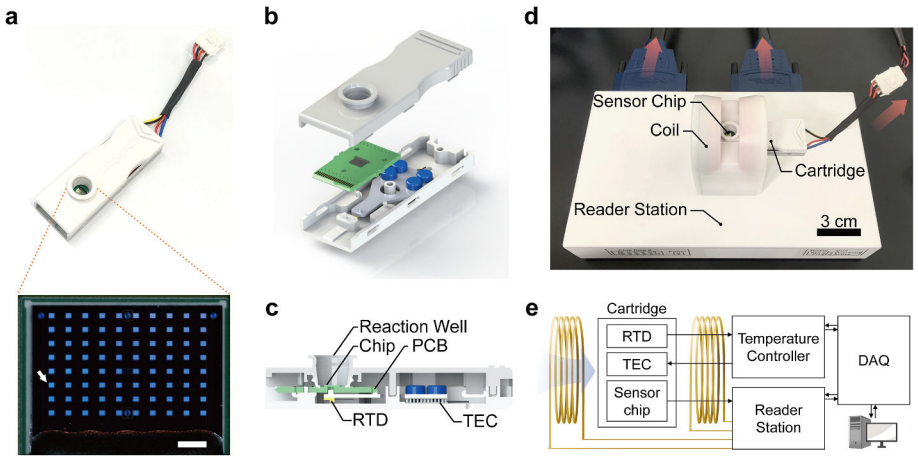

Fig. 1.

GMR biosensors with a built-in temperature modulator. (a) Assembled cartridge and GMR biosensor chip. Blue squares are individual GMR biosensors, and one of them is indicated by an arrow. The scale bar is 500 μm. (b) Exploded view of the custom-designed cartridge and GMR biosensors on a PCB (green). (c) Cross-sectional view of the assembled custom-designed cartridge. (d) A custom-made reader station. The station consists of a Helmholtz coil that can accommodate the cartridge inside and has an opening through which the sensor chip is accessible. The electronics inside are connected to the GMR sensor chip and DAQ boards, and the cartridge is connected to a temperature controller. (e) Schematic of the GMR biosensor system. The Helmholtz coil is used to apply an external magnetic field.

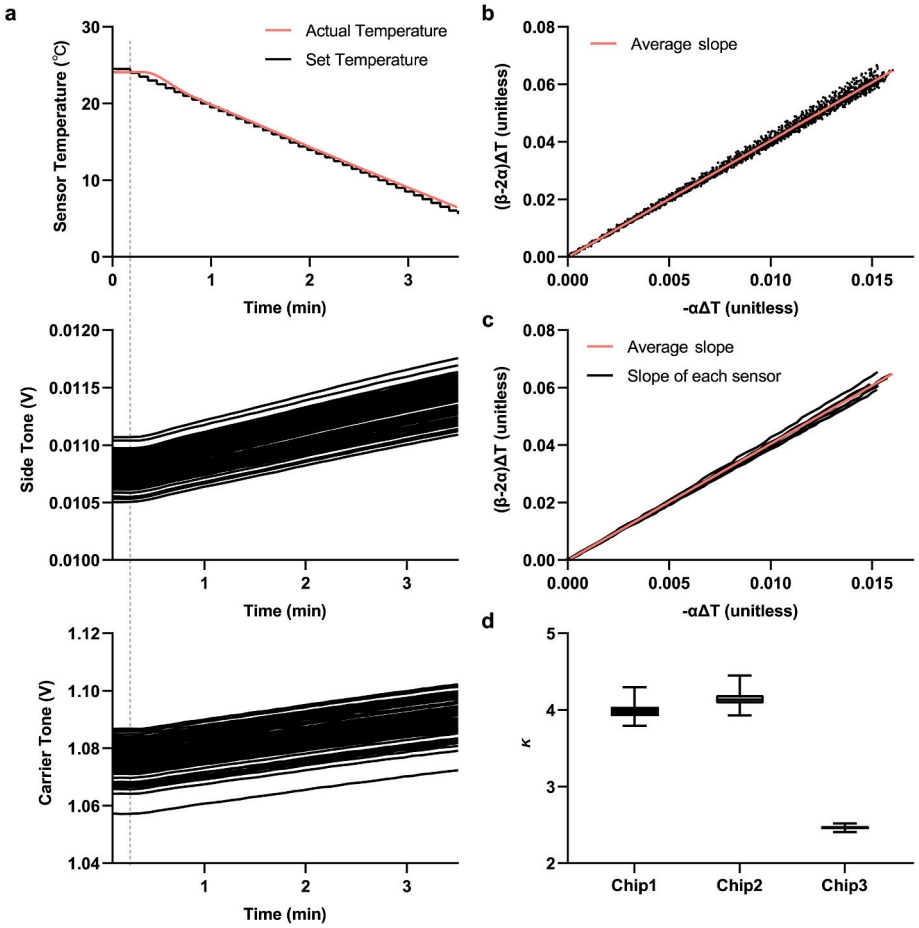

Fig. 2.

(a) Profiles of sensor temperature and ST and CT signals. The dashed line indicates the onset of the temperature sweep. (b) Temperature correction coefficient (the slope in the graph) calculated using signals from all sensors. (c) Variation in temperature correction coefficients of different sensors on the same chip. Only 10 coefficients are plotted together with the averaged coefficient for comparison. (d) Variations in temperature correction coefficients (κ) across sensors on different chips displayed as box and whisker plots. Boxes represent the upper and lower quartiles, and whiskers depict the minimum and maximum of the data without any outliers.

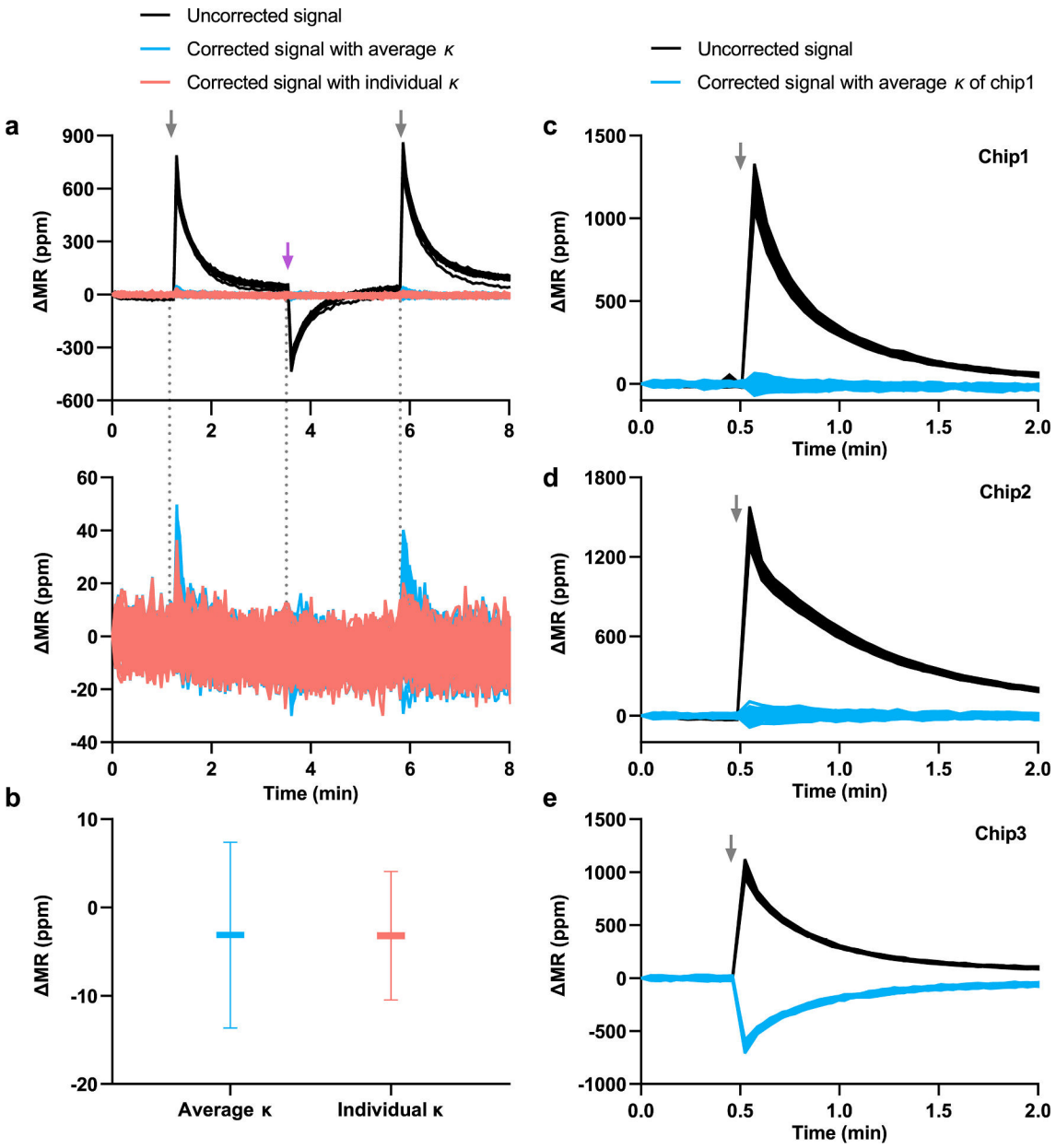

Fig. 3.

(a) Uncorrected signals from 80 sensors (black) and the same signals corrected using either averaged (blue) or individual (red) temperature correction coefficients. The purple and gray arrows indicate the addition of hot water (40 °C) and cold water (4 °C), respectively. To clearly show the difference between averaged and individual temperature correction, only corrected signals are shown at the bottom. (b) Standard deviations (SDs) of 30-s-long signals after the peak corrected using averaged (blue) and individual (red) temperature correction coefficients. Uncorrected and corrected signals from (c) chip1, (d) chip 2, and (e) chip 3 using the average temperature correction coefficient obtained from chip1. The gray arrows indicate the addition of cold water (4 °C).

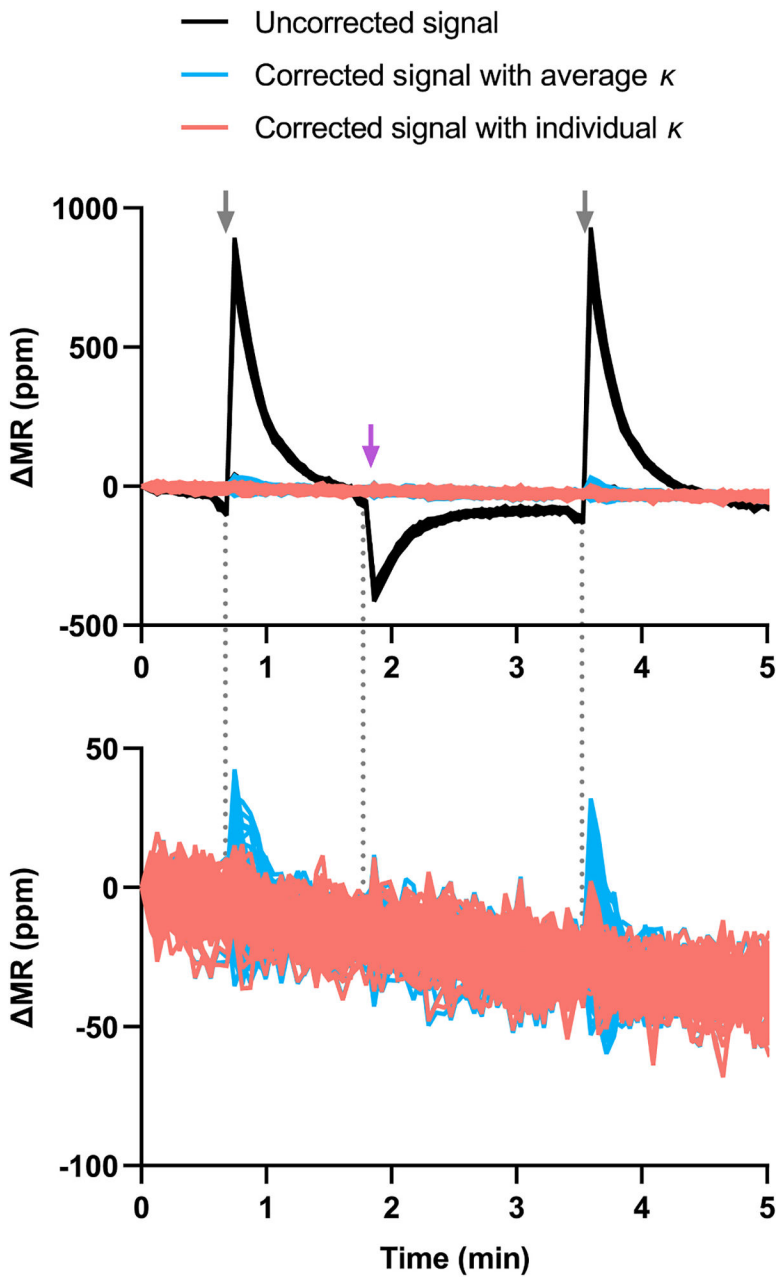

Fig. 4.

Uncorrected signals from 80 sensors (black) with temperature regulated at 30 °C and the same signals corrected using either averaged (blue) or individual (red) temperature correction coefficients. The purple and gray arrows indicate the addition of hot water (40 °C) and cold water (4 °C), respectively. To clearly show the difference between averaged and individual temperature correction, only corrected signals are shown at the bottom.

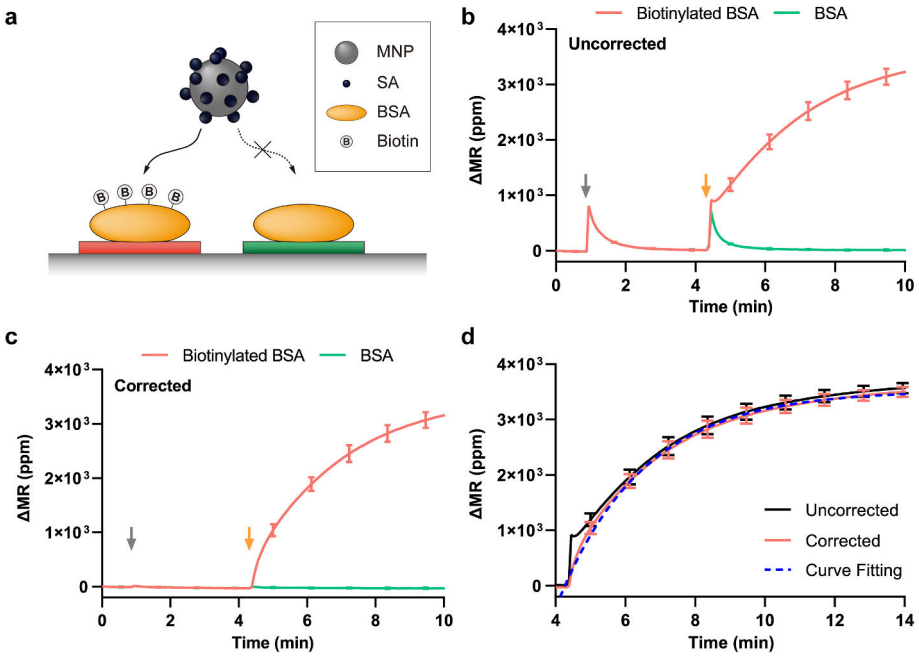

Fig. 5.

Binding curve correction (a) Schematic of MNP binding on the sensors with biotinylated BSA and BSA. SA indicates streptavidin. Average (b) uncorrected and (c) corrected signals from the sensors with biotinylated BSA (red) and BSA (green). The gray and yellow arrows indicate the addition of cold water and cold MNPs, respectively. (d) Curve fitting for binding kinetics. Uncorrected (black) and corrected (red) signals that represent MNP bindings to biotinylated BSA are displayed together with a fitted curve (dashed blue) for the corrected signals. The error bars represent the SD of signals from the sensors with the same probe ($n = 40$).

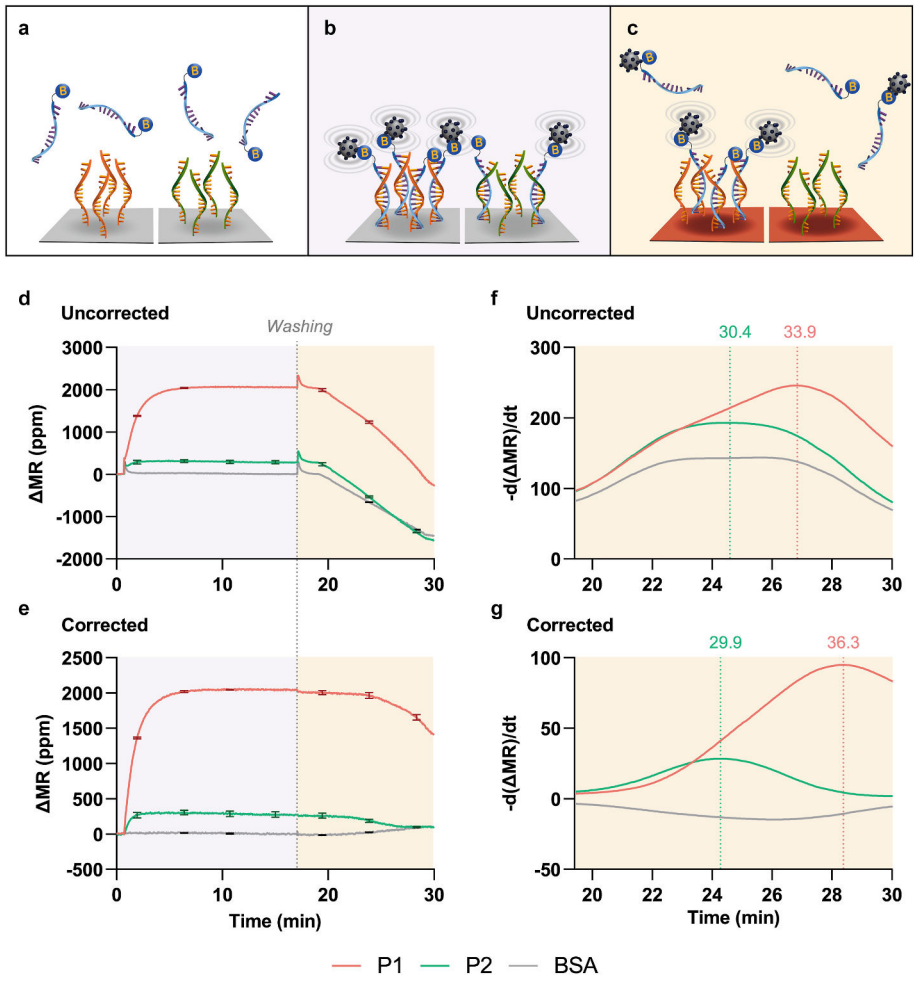

Fig. 6.

(a) Incubation of the target oligonucleotide. Sensors were functionalized with different probe oligonucleotides (P1 and P2) and BSA (not shown). (b) Addition of MNPs. The added MNPs were bound to hybrids on the sensors via the streptavidin-biotin interaction. (c) Melting curve analysis. As the temperatures of the sensors increased, target oligonucleotides together with MNPs were denatured and released from the hybrids. (d) Uncorrected and (e) corrected signals obtained during MNP incubation and melting curve analysis. Green, red, and gray signals represent the average from the replicated sensors with P1, P2, and BSA, respectively. The error bars represent the SD of signals from the sensors with the same probe ($n = 2$). Inverted derivatives of (f) uncorrected and (g) corrected signals during the melting curve analysis. The maximum point of each curve was converted into the corresponding melting temperature.